Isotacticity effect on crystallization and melting in polypropylene fractions: 1. Crystalline structures and thermodynamic property changes

Stephen Z. D. Cheng*, James J. Janimak and Anqiu Zhang
Institute and Department of Polymer Science, College of Polymer Science and Polymer Engineering, The University of Akron, Akron, OH 44325-3909, USA

and Eric T. Hsieh
Research and Development, Phillips Petroleum Company, Bartlesville, OK 74004, USA
(Received 14 December 1989; accepted 28 February 1990)

A set of polypropylene (PP) fractions with similar molecular masses and distributions but different isotacticities have been studied through wide-angle X-ray diffraction, small-angle X-ray scattering and differential scanning calorimetry measurements. The crystal unit-cell parameters, crystallinity, apparent crystal size and lamellar crystal thickness are found to be dependent on crystallization temperature and isotacticity. The equilibrium thermodynamic properties (melting temperature and heat of fusion) for these PP fractions were determined following two extrapolation methods. These fractions can be thought of as stereo-copolymers, with configurational defects along the chains. A uniform inclusion model proposed by Sanchez and Eby can be applied to describe the crystals formed in these fractions. Both equilibrium and non-equilibrium data are discussed.

(Keywords: apparent crystal size; configurational defect; crystal unit cell; crystallinity; heat of fusion; isotacticity; lamellar thickness; melting temperature; polypropylene; thermodynamic property; uniform inclusion model)

INTRODUCTION

The crystallization and the crystalline architecture of isotactic polypropylene (i-PP) from the melt have been interesting topics for the last 30 years or so[1-10]. Besides the regime transitions in i-PP, which have been extensively studied by utilizing the present nucleation theory[11-14], several factors that govern the crystallization behaviour of i-PP have been further discussed. These include the effects of molecular mass and molecular-mass distribution, isotacticity, multiple crystalline structures and branching lamellar morphologies. Just like other vinyl polymers, it is very difficult, from a synthetic point of view, to obtain at the same time both a narrow polydispersity as well as high isotacticity. As a result, the molecular-mass dependence of crystallization in i-PP fractions is not yet well established. On the other hand, the isotacticity effect is also difficult to separate from other factors in the study of i-PP crystallization.

Isotactic polypropylene shows four distinguishable chain conformations with each being a $2 \times 3/1$ helix[15]. Different packing geometries lead to three well known crystalline structures (polymorphs), namely the monoclinic (α) form, the hexagonal (β) form and the triclinic (γ) form. The appearance of these three structures is critically dependent upon the crystallization conditions[15-22]. Among these three crystalline structures, the monoclinic (α) form is by far the most common, being found in normal melt-crystallized or solution-crystallized i-PP samples. Furthermore, it is interesting to note that rapid quenching of i-PP fails to produce totally amorphous samples even when the cooling rate is as high as 10000 K min^{-1} (ref. 23). Natta described this structure as 'smectic', and suggested that it is composed of parallel $2 \times 3/1$ helices but that disorder exists in the packing of the chains perpendicular to their axes[15]. Miller proposed that the quenched form is 'paracrystalline'[24], while Wunderlich classified it as 'conformationally disordered' (condis) crystal[25]. Gailey and Ralston[26] as well as Gezovich and Geil[27] identified that the quenched form consists of very small hexagonal crystallites. Lately, McAllister *et al.* suggested from their X-ray diffraction results that the quenched form represented approximately 60% of the amorphous fraction with the remainder of the sample having the helices arranged in a 'square' array with a cubic or tetragonal symmetry[28]. Recently, Gomez *et al.* have reported that from their high-resolution solid-state ^{13}C nuclear magnetic resonance study the local packings of $2 \times 3/1$ helices are very similar in the β and quenched ('smectic') forms of i-PP[29]. On the other hand, Corradini *et al.* indicated that in quenched i-PP a fairly high correlation of distances is present within each chain and between neighbouring chains to form small bundles. The local correlations between chains are probably nearer to those characterizing the crystal structure of the monoclinic form than to those characterizing the structure of the hexagonal form[30].

The crystalline morphology of i-PP is dominated by a highly characteristic lamellar branching, which has no counterpart in other crystalline polymers. The branching

* To whom correspondence should be addressed

0032-3861/91/040648-08

is observed only for the α form, and not for the β and the γ forms, although all three structures are based on the same $2 \times 3/1$ helical conformation of the chain. It has been recognized that this lamellar branching is characterized by the constant angle between the daughter and mother branches (80° or 100°). The degree of the branching is temperature-dependent. This leads to birefringence changes in spherulites crystallized at different temperatures[1,2,31–37].

In this series of publications, we report our recent study on the crystallization and melting of five PP fractions, which have similar molecular masses and molecular-mass distributions, but different isotacticities. In this paper, we focus on the changes in the crystalline structures and thermodynamic properties in these fractions with respect to the isotacticity and crystallization conditions. The overall crystallization behaviour, linear crystal growth rates, crystal melting and crystalline morphologies will be studied in the following publications of this series.

EXPERIMENTAL

Materials and samples

Five PP fractions, designated as PP(X-20), PP(Y-17), PP(Y-9), PP(X-6) and PP(X-3), were kindly provided by the Phillips Petroleum Co., Bartlesville, Oklahoma. Their molecular characteristics, such as molecular masses, polydispersities and isotacticities, are listed in *Table 1*. Based on high-resolution ^{13}C nuclear magnetic resonance (n.m.r.) data, these PP fractions are predominantly in head-to-tail sequences. The distributions of changing between *d* and *l* configurations are random along the chain backbone. All the fractions are in the molecular-mass range where their thermodynamic properties should not be sensitive to the molecular-mass differences except for the different isotacticities.

The dried PP samples were first heated to 483.2 K for 5 min under vacuum. They were then quickly switched to an oil bath (NESLAB TMV-40DD) at a predetermined crystallization temperature (with an accuracy of ± 0.1 K). After the samples were completely crystallized, they were quenched to room temperature and ready for both wide-angle X-ray diffraction (WAXD) and differential scanning calorimetry (d.s.c.) measurements. For small-angle X-ray scattering (SAXS) experiments, the PP samples were put into aluminium cups, and heated to 483.2 K as before. The samples were then quickly switched to a hot stage on the X-ray apparatus at predetermined temperatures. The SAXS data were obtained after complete crystallization. The times for complete crystallization were determined via d.s.c. isothermal crystallization experiments.

Instrumentation and experiments

Wide-angle X-ray diffraction (WAXD) and small-angle X-ray scattering (SAXS) experiments were conducted with a Rigaku 12 kW rotating-anode generator as the source of the incident X-ray beam. The point-focused beams were monochromatized with a graphite crystal to ensure Cu K_α radiation. For the WAXD experiments, the Rigaku powder diffractometer (D/Max-B) was used to measure diffraction intensity *versus* 2θ. The calibration of these WAXD measurements was carried out by applying standard materials. The crystallinity determination was conducted by following Ruland's method[38] in a diffraction angle (2θ) range between 8° and 90°. The apparent crystal sizes were calculated by the following Scherrer equation:

$$L(hkl) = A/(\delta s)_s$$

where the constant A is geometry-dependent and has for its chosen units a value of unity, and $(\delta s)_s$ is the breadth at half-height expressed in units of s in $Å^{-1}$ (ref. 39).

For the SAXS experiments, a Rigaku SAXS goniometer was modified with a 505 mm vacuum chamber. A Braun OED 50 mm position-sensitive detector was attached. Lorentz corrections of the SAXS data were conducted by multiplying the intensity, I (counts per second), with s^2 ($s = 2 \sin\theta/\lambda$ where λ is the X-ray wavelength, 1.54178 Å). The crystal lamellar thickness was calculated by following Strobl's correlation function method[40]. For our SAXS experiments, a scattered photon accumulation of about 2 min was sufficiently strong for data acquisition.

A DuPont 9900 thermal analysis system was used for d.s.c. measurements. After the PP samples were measured in WAXD, a small portion weighing about 1 mg from each sample was used to observe its melting behaviour. The heating curves were recorded at a heating rate of 10 K min^{-1}. All melting temperatures for the d.s.c. results quoted in this paper refer to thermal lag-corrected onset temperatures. The calorimeter was calibrated according to the standard procedures established in our laboratory.

Table 1 Molecular characteristics of the PP fractions with different isotacticities

Assignment	$\bar{M}_w \times 10^{-3}$	$\bar{M}_w/\bar{M}_n$	Isotacticity
PP(X-20)	202	2.6	0.988
PP(Y-17)	159	2.3	0.978
PP(Y-9)	189	3.0	0.953
PP(X-6)	209	1.8	0.882
PP(X-3)	190	1.6	0.787

RESULTS

Crystalline structure

Figure 1 shows the relationship between the WAXD intensity and the diffraction angle 2θ for the five PP fractions, PP(X-20), PP(Y-17), PP(Y-9), PP(X-6) and PP(X-3), crystallized at 429.2, 428.2, 416.2, 393.2 and 376.2 K, respectively. Three structure parameters can be obtained; namely, the crystal unit-cell structure, the weight fraction crystallinity and the apparent crystal size normal to particular crystal planes. Qualitatively, on decreasing the isotacticity of the PP fractions, one can clearly observe that the intensities of these diffraction peaks decrease when compared with the amorphous halos. Simultaneously, the half-heights of these diffraction peaks increase. The angle positions (2θ) of these diffraction peaks are also shifted to lower values. Quantitatively, two avenues of study become immediately apparent: first, for a particular PP sample with a certain isotacticity content, these three structure parameters change with supercooling (crystallization temperature); and secondly, for a fixed supercooling, these three structure parameters change with isotacticity. *Figures 2–4* show these relationships. It is evident that, from *Figure 2*, the crystal unit-cell size and angle (β)

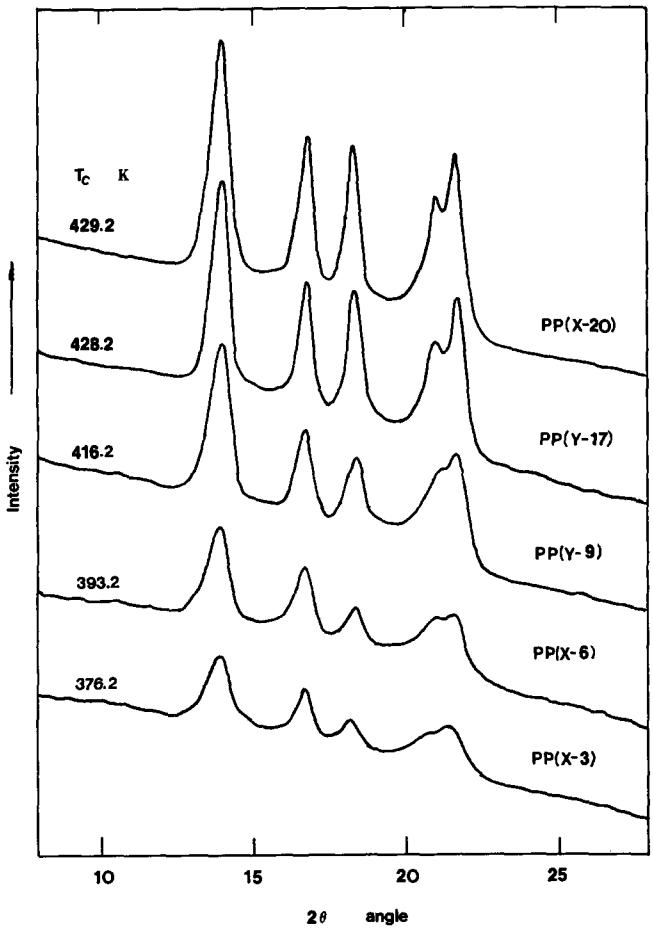

Figure 1 WAXD powder patterns for the PP fractions with different isotacticities crystallized at different crystallization temperatures

change with supercooling for two PP fractions (PP(X-20) and PP(X-3)), which serve as two extreme cases. In this supercooling region ($\Delta T = 20$–90 K), all unit cells for these PP fractions show monoclinic structures. The changes in the unit-cell size and angle (β) for the PP(X-3) fraction are smaller than those changes in the PP(X-20) fraction. For instance, the a axis of the unit cell of the PP(X-3) fraction decreases from 0.683 nm at $\Delta T = 83$ K to 0.679 nm at $\Delta T = 28$ K. Its counterpart for the PP(X-20) fraction changes from 0.678 to 0.670 nm in the same supercooling region. The b axis changes from 2.122 to 2.116 nm and from 2.118 to 2.109 nm for these two fractions, respectively. The c axis, however, is essentially unchanged, as 0.655 ± 0.001 nm. The angle β, on the other hand, changes from 98.5° at $\Delta T = 83$ K to 98.8° at $\Delta T = 28$ K for the PP(X-3) fraction and from 98.8° at $\Delta T = 83$ K to 99.2° at $\Delta T = 20$ K for the PP(X-20) fraction. A clear tendency of the analogous changes of these unit-cell sizes and angles for other PP fractions can also be observed.

Crystallinity and crystal size

Figure 3 indicates the changes in crystallinity as determined by X-ray diffraction of these PP fractions with different supercoolings (crystallization temperatures). For all fractions, their crystallinities increase with decreasing supercooling. Nevertheless, for the PP(X-3) fraction with low isotacticity, this increase is limited. Its total crystallinity is also low (<25%). For the PP(X-20) fraction, which has 98.8% isotacticity, on the other hand, the crystallinity increases to as high as 65%. At a constant supercooling, it is interesting that the crystallinity exhibits approximately an exponential dependence with isotacticity. Using the Scherrer equation described in the

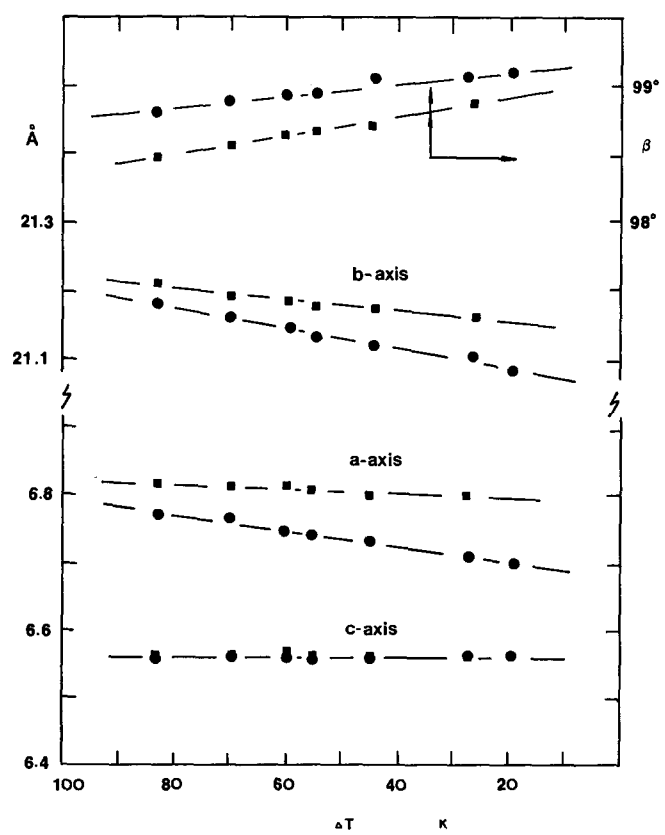

Figure 2 The crystal unit-cell parameters (a, b, c and β) for PP(X-20) (●), and PP(X-3) (■) change with supercooling

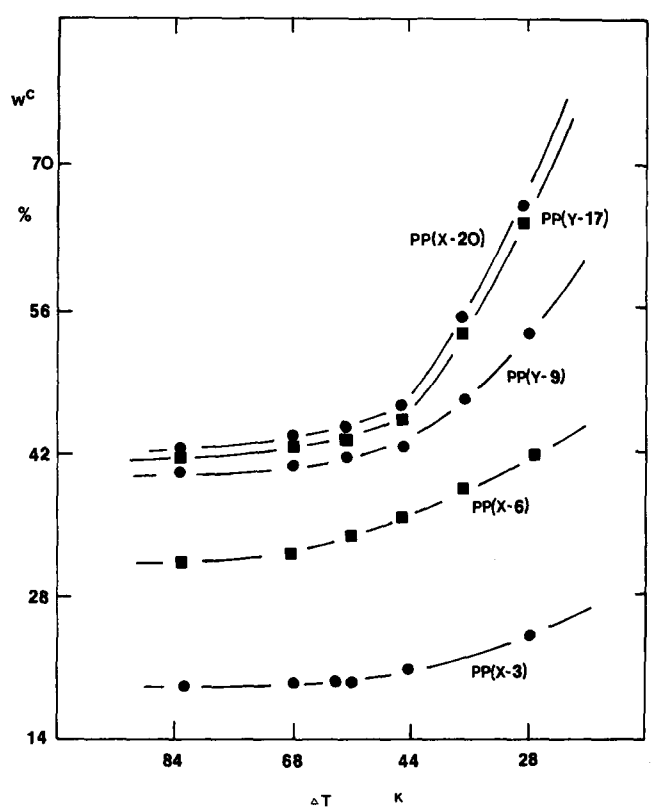

Figure 3 Relationships between crystallinity and supercooling for the PP fractions with different isotacticities

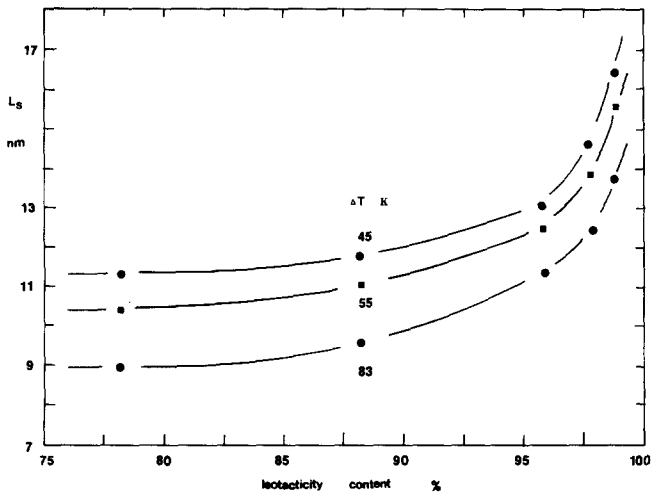

Figure 4 Relationships between apparent crystal size and supercooling for the PP fractions with different isotacticities

'Experimental' section, one can only calculate relative values of the apparent crystal size normal to a particular crystal plane, such as shown in *Figure 4*, for the (1 1 0) plane. However, it is clear that the apparent crystal size increases with isotacticity and crystallization temperature, in particular, at higher isotacticity and temperature (low supercooling). Along other crystal planes, similar situations can also be observed.

Lamellar crystal thickness

Table 2 lists the SAXS results for the PP fractions, which were crystallized at different crystallization temperatures. It is obvious that the lamellar thickness of the crystals decreases with isotacticity for a given supercooling (the same supercooling means different crystallization temperatures due to different T_m°; see below). For example, at $\Delta T = 42$ K, the lamellar thickness of the PP(X-20) fraction is 13.1 nm, while that of the PP(Y-9) fraction is 12.6 nm. For the PP(X-6) fraction, the thickness is only 10.9 nm. On the other hand, the lamellar thickness for each fraction increases with decreasing supercooling. Nevertheless, the lamellar thickness of these fractions at a constant temperature shows an interesting tendency. Namely, with decreasing isotacticity, the thickness seems to increase, instead of decrease, as one often suspects, as shown in *Table 2*.

Furthermore, the width of the SAXS peaks for the PP(X-20) fraction is about three times as narrow as that for the PP(X-3) fraction at the same ΔT, indicating different distributions of the long-spacing sizes for these fractions with different isotacticities.

Equilibrium melting temperatures

Our d.s.c. results indicate that all these PP fractions crystallized in this supercooling region ($\Delta T = 20$–90 K) show two distinguishable melting peaks. The high melting peak is usually formed first, followed by the development of the low melting peak. With decreasing supercooling, the heat of fusion of the high melting peak is reduced, and both melting peaks shift towards higher temperatures. Nevertheless, the low melting peak increases in temperature faster than the high melting peak for all of these fractions. If one plots the onset melting temperatures of the low melting peaks with respect to the isothermal crystallization temperatures, as shown in *Figure 5*, the equilibrium melting temperatures of these fractions with different isotacticities may be obtained. From this figure, the extrapolations of the melting temperatures were observed to cross over the 45° line of $T_m = T_c$ yielding 457.4, 455.5, 453.0, 446.5 and 436.6 K, for these PP fractions, respectively.

Combining the lamellar thicknesses with our d.s.c. measurements of the melting temperatures for these PP fractions, we can also obtain the equilibrium melting temperatures for each fraction by extrapolating the reciprocal lamellar thickness to zero. *Figure 6* shows these relationships for these five fractions. The equilibrium melting temperatures for these fractions are 457.6, 456.4, 453.7, 445.8 and 435.7 K, respectively. Since these

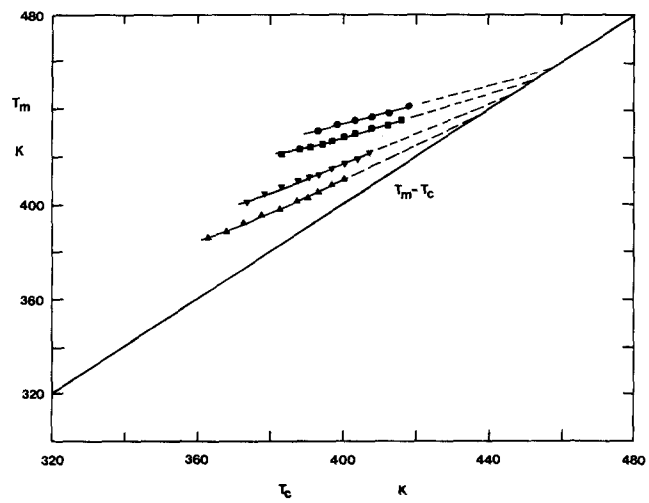

Figure 5 Equilibrium melting temperature determinations for the PP fractions with different isotacticities based on extrapolations from the T_c *versus* T_m plots. ●, PP(Y-17); ■, PP(Y-9); ▼, PP(X-6); ▲, PP(X-3)

Table 2 Lamellar thickness of the PP fractions with different isotacticities crystallized from the melt

Assignment	T_c (K)	L_{exp}[a] (nm)	l_{exp} (nm)
PP(X-20)	385	19.2	8.4
	395	21.5	9.9
	405	22.4	10.8
	415	25.7	13.1
	425	30.4	20.1
PP(X-17)	380	20.7	8.3
	390	21.9	9.0
	400	22.8	9.8
	410	25.1	11.8
	420	30.1	18.1
PP(Y-9)	380	23.1	8.3
	390	24.8	9.2
	400	26.9	10.8
	410	29.4	12.6
	420	32.5	18.2
PP(X-6)	360	20.2	6.3
	370	22.2	7.0
	380	25.5	8.4
	390	27.0	9.3
	400	29.5	10.9
PP(X-3)	335	24.6	4.4
	345	24.7	4.7
	355	29.0	5.8
	365	31.4	6.6
	375	35.0	7.7

[a] L_{exp} represents the long spacing observed via SAXS measurements

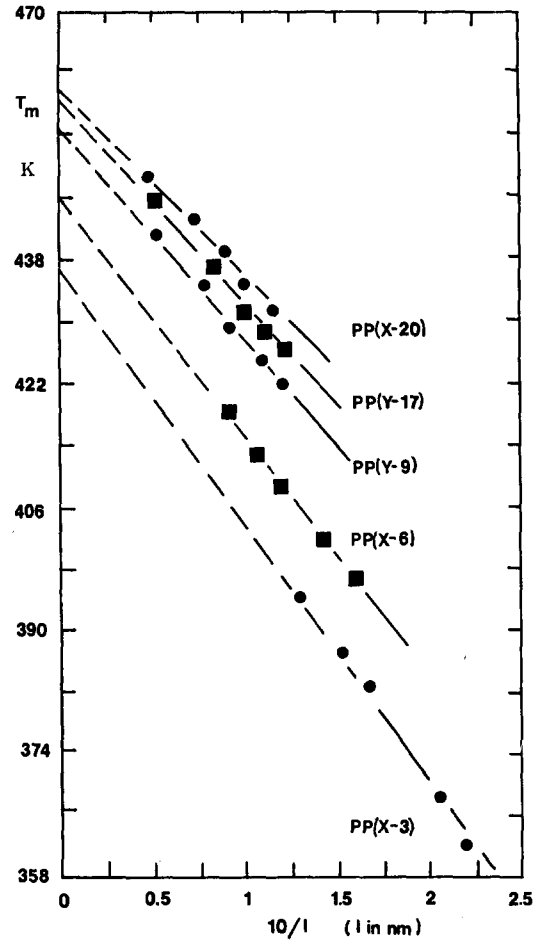

Figure 6 Equilibrium melting temperature determinations for the PP fractions with different isotacticities based on extrapolation from the T_m *versus* $1/l$ plots

extrapolations are based on the Thomson–Gibbs equation (see below), the slopes of these linear relationships should represent the fold surface free energy, σ_e, for these PP fractions. Nevertheless, the Thomson–Gibbs equation has to be modified when one deals with stereo-copolymers such as these PP fractions. This condition is up-rooted since the fold surface free energy and the latent heat of fusion may vary in a significant manner. Since the molecular mass is relatively high, end-groups probably are a very minor component to the fold surface free energy. A detailed discussion of this topic will be given in the next section. The absolute values of these slopes are -2.411×10^{-4}, -2.538×10^{-4}, -2.805×10^{-4}, -3.075×10^{-4} and -3.396×10^{-4} nm K, respectively.

Equilibrium heat of fusion

Based on our crystallinity determinations from WAXD experiments and the heat of fusion data obtained via d.s.c. measurements, we can calculate the equilibrium heat of fusion for these PP fractions with 100% crystallinity at different isotacticities. Within an average deviation of $\pm 5\%$, we have 8.68, 8.66, 8.59, 8.45 and 8.29 kJ mol^{-1} for each fraction, respectively. It is clear that, with decreasing isotacticity, the equilibrium heats of fusion decrease in this series of PP fractions. On the other hand, one can also plot the relationship between the heat of fusion and the crystallization temperature. The extrapolations may be conducted similar to the case of *Figure 5*. Nevertheless, the extrapolations generate a larger deviation ($\pm 10\%$). Their average values are 8.70, 8.69, 8.61, 8.48 and 8.26 kJ mol^{-1} for these PP fractions, respectively. However, a tendency of the equilibrium heat of fusion to decrease with isotacticity is evident. *Table 3* lists to a best approximation the equilibrium data for these PP fractions.

DISCUSSION

This series of PP fractions can be recognized as random stereo-copolymers. The isotacticities listed in *Table 1* can be understood by the way in which the chain molecules are disturbed by different configurations with respect to the methyl groups by certain degrees of probability. For instance, in the case of PP(X-20) with an isotacticity of 98.8%, the chain molecules statistically show an interruption by an opposite configuration after every 83.3 isotactic repeat units for every 100 repeat units sampled. On decreasing isotacticity to 78.7% in the PP(X-3), the number of isotactic repeat units now statistically decreases to 4.7. These interruptions act as point defects in the chain conformation. After these interruptions the original chain configuration is recovered. On the other hand, based on n.m.r. studies, the PP fractions are predominantly in head-to-tail sequences. The defects introduced due to isoclined and anticlined configurations with respect to the methyl groups within one chain molecule (in a visible description, the helices in which the methyl group points either 'up' or 'down' relative to the crystallographic c axis) should not be a major effect in this study. This series of PP fractions with different isotacticities thus serves as a good example to study crystallization and melting behaviour of the random stereo-copolymers.

Theories of random copolymer crystallization have been developed for the melting temperature[41–45], the kinetics of crystallization[42,44] and the amount of non-crystallizable comonomer that is incorporated into the crystalline phase[43]. Two extreme cases are usually discussed: uniform inclusion and complete exclusion of comonomers. The former can be described as the crystalline phase of a solid solution for both comonomers (A and B); the B comonomers produce defects in the crystalline A lattice and both crystalline and amorphous phases have the same composition. The latter is concerned with the crystalline phase being composed entirely of A comonomers and in metastable equilibrium with a mixed amorphous phase of A comonomers and non-crystallizable B comonomers. Following thermodynamics, let X mole fraction be the overall fraction of B comonomers in the random copolymer. The probability that m units in a chain of n units will be B comonomers is given by a binomial distribution:

$$P(m) = [n!/m!(n-m)!]X^m(1-X)^{n-m} \quad (1)$$

Table 3 Thermodynamic data for the PP fractions with different isotacticities

Assignment (kJ mol^{-1})	T_m (K)	ΔH_f (kJ mol^{-1})	ε
PP(X-20)	457.0	8.68	1.90
PP(Y-17)	456.0	8.66	1.90
PP(Y-9)	453.4	8.61	1.94
PP(Y-6)	446.2	8.47	1.93
PP(X-3)	436.2	8.28	1.96

The partition function is given by Helfand and Lauritzen[43]:

$$Q = \sum_{m=0}^{n} P(m) \exp(-\beta m\varepsilon) = \sum_{m=0}^{n} q(m)$$
$$= [1 - X + X \exp(-\beta\varepsilon)]^n \quad (2)$$

where $\beta = 1/kT$. The term $q(m)$ in the partition function is representative of a metastable state, and the maximum term corresponds to the equilibrium state. The change in Gibbs free energy between a metastable crystal of concentration $X_c = M_c/n$ and the melt is thus derived by Sanchez and Eby[44] as:

$$\Delta G = \Delta G^\circ + RT \ln q(M_c) \quad (3)$$

$$\Delta G = \Delta G^\circ - RT\left[\frac{X_c\varepsilon}{RT} + (1 - X_c)\ln\left(\frac{1 - X_c}{1 - X}\right) + X_c \ln\left(\frac{X_c}{X}\right)\right]$$

where $\Delta G^\circ = \Delta H_f^\circ(1 - T/T_m^\circ)$ is the change of Gibbs free energy, T_m° is the equilibrium melting point and ΔH_f° is the equilibrium heat of fusion of the homopolymer with A comonomers. The excess energy of the defects created by the incorporation of a mole of B comonomer in the crystalline A lattice is ε.

Setting $\Delta G = 0$ in equation (3) yields the melting temperature T_m of an infinitely large crystal of crystalline composition X_c:

$$\frac{1}{T_m} - \frac{1}{T_m^\circ} = \frac{R}{\Delta H_f^\circ}\left[\frac{X_c\varepsilon}{RT_m} + (1 - X_c)\ln\left(\frac{1 - X_c}{1 - X}\right) + X_c \ln\left(\frac{X_c}{X}\right)\right] \quad (4)$$

When $X_c = 0$, equation (4) reduces to the Flory equation[41] for the exclusion model:

$$\frac{1}{T_m^\circ} - \frac{1}{T_m} = \frac{R}{\Delta H_f^\circ}\ln(1 - X) \quad (5)$$

When $X_c = X$, equation (4) reduces to that for the uniform inclusion model:

$$T_m = T_m^\circ(1 - X\varepsilon/\Delta H_f^\circ) \quad (6)$$

When $X_c = X_{eq}$, equation (4) reduces to the form for an equilibrium number of defects[44]:

$$\frac{1}{T_m^\circ} - \frac{1}{T_m} = \frac{R}{\Delta H_f^\circ}\ln[1 - X + X \exp(-\beta\varepsilon)] \quad (7)$$

It is evident that the term $\beta\varepsilon$ plays an important role for the inclusion or exclusion models. If $\beta\varepsilon$ is large, exclusion of comonomers occurs since the term $X \exp(-\beta\varepsilon)$ approaches zero and equation (7) reduces to equation (5). If $\beta\varepsilon$ is small ($\ll 1$), the inclusion model works. It has to be emphasized that these equations were derived under the assumptions of equilibrium thermodynamics.

Since we have obtained the equilibrium melting temperatures for these PP fractions, one would like to compare the experimentally extrapolated data with theoretical calculations for these three models. First, for the complete exclusion model based on equation (5) (let T_m° of the i-PP homopolymer be 458.2 K, ΔH_f° be 8.70 kJ mol^{-1}), one can calculate that the melting temperature depression for the PP(X-3) fraction can be as high as 44 K; namely, a melting temperature of 414.7 K should be obtained through extrapolation. Nevertheless, the highest melting temperature we observed experimentally for this fraction is 412 K at $T_c = 400$ K. Our extrapolated data for T_m of this fraction are about 20 K higher than this calculated value, indicating that to at least some degree comonomer inclusion occurs in these PP fractions during crystallization. If one applies the model involving the equilibrium number of defects as described in equation (7), one can actually calculate the excess energy ε from the equilibrium melting data. However, one cannot get the numerical values of both the PP(X-20) and the PP(Y-17) fractions since the equations do not generate solutions with real values. For the other three PP fractions, ε varies from about 3 to 15 kJ mol^{-1}, which is much too large for the upper limit (15 kJ mol^{-1}) when compared with the equilibrium heat of fusion of the i-PP polymer (8.70 kJ mol^{-1}). On the other hand, using the uniform inclusion model based on equation (6), one can calculate the excess energy ε for these fractions; the values are quite close to each other, ranging from 1.90 kJ mol^{-1} for the PP(X-20) fraction to 1.96 kJ mol^{-1} for the PP(X-3) fraction. These values represent three-fifths of the excess energy values for copolymers of tetrafluoroethylene and hexafluoropropylene[46]. Since these PP fractions are only considered as stereo-copolymers, no different chemical repeat units are involved. One may expect a lower excess energy ε in these cases. Another example is the copolymers of L- and DL-lactides[47]. The excess energy ε for this system is 2.45 kJ mol^{-1}, which is indeed lower than the former copolymer system[46].

Correspondingly, the experimental equilibrium heats of fusion for the PP fractions decrease with isotacticity. They follow the equation:

$$\Delta H_f(X, T_m) = \Delta H_f^\circ - \varepsilon X \quad (8)$$

Combining this with the equilibrium melting temperature data, the equilibrium entropy changes for these fractions at their melting temperatures are essentially unchanged (the equilibrium entropy change for i-PP with 100% isotacticity is 18.88 J K^{-1} mol^{-1}).

Unfortunately, as usual for crystal melting in semicrystalline polymeric systems, these PP fractions reveal non-equilibrium crystal melting behaviour. The crystals are generally of small size (at least in one dimension, such as lamellar crystals) and contain defects. For the copolymer with lamellar crystals, one can incorporate equation (4) with the expression $\Delta G - 2\sigma_e/l = 0$. Under the condition of the inclusion model, one has:

$$T_m(l) = T_m^\circ\left(1 - \frac{2\sigma_e}{\Delta H_f^\circ l} - \frac{\varepsilon X}{\Delta H_f^\circ}\right) \quad (9)$$

Substituting equation (6) into equation (9), one obtains:

$$T_m(l) = T_m - \frac{2\sigma_e T_m^\circ}{\Delta H_f^\circ l} \quad (10)$$

Therefore, the linear extrapolations between the melting temperature and reciprocal lamellar thickness made in *Figure 6* are essentially representative of this equation (equation (10)). The intersection on the temperature scale at $1/l = 0$ is T_m, and the slope of the linear relationship is $2\sigma_e T_m^\circ/\Delta H_f^\circ$. The extrapolated T_m data for these PP fractions correspond well to the equilibrium melting temperatures extrapolated based on the T_m *versus* T_c plot

(± 1 K in standard deviation). Based on equation (10), one can also calculate the fold surface free energy, σ_e, for these PP fractions through the values of the slopes shown in *Figure 6*. The values of the fold surface free energies for these fractions are 50.9 erg cm^{-2} for PP(X-20), 53.6 erg cm^{-2} for PP(Y-17), 59.3 erg cm^{-2} for PP(Y-9), 65.0 erg cm^{-2} for PP(X-6) and 71.8 erg cm^{-2} for PP(X-3). It is evident that, with decreasing isotacticity in these PP fractions, the fold surface free energy increases. Nevertheless, this increase in the fold surface free energy may also be obscured by two effects: first, the lateral crystal size in the PP fractions decreases with lowering isotacticity, and therefore the lateral surface free energy can no longer be neglected (see *Figure 4*); and secondly, the expansion of the crystal lattice along both *a* and *b* axes (*Figure 2*) leads to a decrease of the number of folds per unit area of fold surface. We cannot at this moment quantitatively separate these two effects from the slope values.

From the change in unit-cell parameters with supercooling for the PP(X-3) fraction (*Figure 2*), it is evident that supercooling has only a minor influence in these changes. No matter how much opportunity the molecules have (large chain mobility and long crystallization time) the PP(X-3) fraction crystallizes as a stereo-copolymer with defects. As a consequence, the size of the unit cell does not decrease much with supercooling. A hypothetical length of 4.7 isotactic repeat units is too short to form crystals that only contain the isotactic units. If one compares this length with the lamellar thickness measured by SAXS (*Table 2*), cocrystallization of these units with configurational defects has to take place. On the other hand, for the PP(X-20) fraction, the change of the unit-cell parameters with supercooling is relatively large, indicating that more regular crystals can form at low supercoolings where the chain molecules may adjust themselves to more energetically favourable positions. However, even at the lowest supercooling we studied here ($\Delta T = 20$ K) the unit-cell parameters are still much larger than the reported i-PP data[48]. For instance, the *a* axis for the PP(X-20) fraction at $\Delta T = 20$ K is 0.670 nm compared with $a = 0.665$ nm for i-PP; the *b* axis is 2.109 nm compared with $b = 2.096$ nm for i-PP; and the β angle is 99.3° compared with $\beta = 99.62°$ for i-PP. Furthermore, the lamellar thickness listed in *Table 2* at $\Delta T = 32$ K for the PP(X-20) fraction is 20.1 nm. This value is about 1.1 times larger than the length of 83.3 isotactic repeat units (~ 18.0 nm). On the basis of these analyses, one may conclude that, even in the case of the PP(X-20) fraction, the highest isotacticity content studied, at low supercooling the inclusion of configurational defects in the crystals has still taken place. Any polymer crystallization process has been recognized as a process that compromises the thermodynamic driving force and the kinetic pathway. In these PP fractions, the excess energy of the configurational defects is relatively small compared with other random copolymers that have two comonomers with different chemical structures. Following the treatment of Sanchez and Eby[42], when the nucleation theory is applied to this process, the theoretical lamellar crystal thickness is given by[11–14]:

$$l^* = l_c + \delta l \tag{11}$$

where $l_c = 2\sigma_e/\Delta G$ is the critical lamellar crystal thickness and δl is approximately $kT/b_0\sigma$ in the simplest approximation (k is the Boltzmann constant, b_0 is the thickness of a single molecular layer in the crystal and σ is the lateral surface free energy). This term is usually much smaller than l^* (typically about 1.0–1.5 nm). From experimental observations, the lamellar crystal thickness l_{exp} may differ from l^* because crystals may thicken with time. In general:

$$l_{exp} = l_c + C(T_c) \tag{12}$$

where $C(T_c)$ includes δl plus any thickening process at the crystallization temperature T_c. Also $C(T_c)$ is a function of time, but it will be assumed throughout that we are dealing with a long-time value of $C(T_c)$. A further assumption is made that this term is independent of isotacticity (X). One thus has:

$$l_{exp} = l^\circ_{exp} + l^\circ_c f(X, T_c) \tag{13}$$

with

$$f(X, T_c) = \varepsilon X T^\circ_m / (\Delta H^\circ_f \Delta T - \varepsilon X T^\circ_m) \tag{14}$$

where $\Delta T = T^\circ_m - T_c$. When one plots l_{exp} *versus* $f(X, T_c)$ at different T_c, one expects to see linear relationships with intercept $l^\circ_{exp}(T_c)$ and positive slope $l^\circ_c(T_c)$. In these PP fractions, therefore, the theory predicts that, at the same crystallization temperature, the lamellar crystal thickness increases with decreasing isotacticity. Our experimental data listed in *Table 2* indicate that such a relationship exists.

CONCLUSIONS

We have measured the changes in crystal unit-cell parameters, crystallinities and apparent crystal size of five PP fractions containing different isotacticities (78.7–98.8%). Their equilibrium thermodynamic properties have been determined via d.s.c., WAXD and SAXS measurements. All the experimental results indicate that the crystallization process of these PP fractions is kinetically controlled. They can be represented as stereo-copolymers with configurational defects in the chain. The uniform inclusion model in copolymer crystallization proposed by Sanchez and Eby can be applied to describe the experimental observations and the extrapolated equilibrium data.

ACKNOWLEDGEMENT

This work was partially supported by Exxon Educational Foundation.

REFERENCES

1 Padden, F. J. Jr and Keith, H. D. *J. Appl. Phys.* 1959, **30**, 1479
2 Binsberger, F. L. and DeLange, B. G. M. *Polymer* 1968, **9**, 23; 1970, **11**, 309
3 Lovinger, A. J., Chua, J. D. and Gryte, L. C. *J. Polym. Sci., Polym. Phys. Edn.* 1977, **15**, 641
4 Goldfarb, L. *Makromol. Chem.* 1978, **179**, 2297
5 Wlochowicz, A. and Eder, M. *Polymer* 1981, **22**, 1285
6 Martuscelli, E., Silvestre, C. and Abate, G. *Polymer* 1982, **23**, 229
7 Clark, E. J. and Hoffman, J. D. *Macromolecules* 1984, **17**, 878
8 Allen, R. C. and Mandelkern, L. *Polym. Bull.* 1987, **17**, 473
9 Campbell, R. A. and Phillips, P. J. *Bull. Am. Phys. Soc.* 1988, **33**, 546; 1989, **34**, 754
10 Cheng, S. Z. D., Janimak, J. J., Zhang, A.-Q. and Cheng, H. N. *Macromolecules* 1990, **23**, 298
11 Hoffman, J. D., Frolen, L. J., Ross, G. R. and Lauritzen, J. I. Jr *J. Res. Natl. Bur. Std. (A)* 1975, **79**, 671
12 Lauritzen, J. I. Jr *J. Appl. Phys.* 1973, **44**, 4353; see also Lauritzen, J. I. Jr and Hoffman, J. D. *J. Appl. Phys.* 1973, **44**, 4340

13 Hoffman, J. D. *Polymer* 1982, **23**, 656; 1983, **24**, 3
14 Hoffman, J. D. and Miller, R. L. *Macromolecules* 1988, **21**, 3098
15 Natta, G. and Corradini, P. *Nuovo Cim., Suppl.* 1960, **15**, 40
16 Turner-Jones, A., Aizlewood, J. M. and Beckett, D. R. *Makromol. Chem.* 1964, **75**, 134
17 Keith, H. D., Padden, F. J. Jr, Walker, N. M. and Wyckoff, H. W. *J. Appl. Phys.* 1959, **30**, 1485
18 Addink, E. J. and Beintema, J. *Polymer* 1961, **2**, 185
19 Pae, K. D., Sauer, J. A. and Morrow, D. R. *Nature* 1966, **211**, 514
20 Kardos, J. L., Christiansen, A. W. and Baer, E. *J. Polym. Sci. (A-2)* 1966, **4**, 777
21 Lotz, B. and Wittmann, J. C. *J. Polym. Sci., Polym. Phys. Edn.* 1986, **24**, 1541, 1559
22 Lotz, B., Graff, S. and Wittmann, J. C. *J. Polym. Sci., Polym. Phys. Edn.* 1986, **24**, 2017
23 Wu, Z.-Q., Veronica, D. L., Cheng, S. Z. D. and Wunderlich, B. *J. Thermal Anal.* 1988, **34**, 105
24 Miller, R. L. *Polymer* 1960, **1**, 135
25 Wunderlich, B. and Grebowicz, J. *Adv. Polym. Sci.* 1984, **60/61**, 1; see also *Adv. Polym. Sci.* 1988, **87**, 1
26 Gailey, J. A. and Talston, R. H. *SPE Trans.* 1964, **4**, 29
27 Gezovich, D. M. and Geil, P. H. *Polym. Eng. Sci.* 1968, **8**, 202
28 McAllister, P. B., Carter, T. J. and Hinde, R. M. *J. Polym. Sci., Polym. Phys. Edn.* 1978, **16**, 49
29 Gomez, M. A., Tanaka, H. and Tonelli, A. E. *Polymer* 1987, **28**, 2227
30 Corradini, P., Petraccone, V., De Rosa, C. and Guerra, G. *Macromolecules* 1986, **19**, 2699
31 Khoury, F. *J. Res. Natl. Bur. Std. (A)* 1966, **70**, 29
32 Geil, P. H. 'Polymer Single Crystals', Interscience, New York, 1963
33 Morrow, D. R. and Newman, B. A. *J. Appl. Phys.* 1986, **39**, 4944
34 Padden, F. J. Jr and Keith, H. D. *J. Appl. Phys.* 1966, **37**, 4013; 1973, **44**, 1217
35 Lovinger, A. J. *J. Polym. Sci., Polym. Phys. Edn.* 1983, **21**, 97
36 Bassett, D. C. and Olley, R. H. *Polymer* 1984, **25**, 935; 1989, **30**, 399
37 Norton, D. R. and Keller, A. *Polymer* 1985, **26**, 704
38 Ruland, W. and Dewaelheyns, A. *J. Sci. Instrum.* 1966, **44**, 236; *Faserforsch. Textiltechnik* 1967, **18** (2), 59
39 Scherrer, P. *Nachr. Ges. Wiss. Gottingen* 1918, 98; in 'Kolloidchemie' (Ed. R. Zsigmondy), Spamer, Leipzig, 1920
40 Tanabe, Y., Strobl, G. R. and Fischer, E. W. *Polymer* 1986, **27**, 1147
41 Flory, P. J. *Trans. Faraday Soc.* 1955, **51**, 848
42 Sanchez, I. C. and Eby, R. K. *J. Res. Natl. Bur. Std. (A)* 1973, **77**, 353
43 Helfand, E. and Lauritzen, J. I. Jr *Macromolecules* 1973, **6**, 631
44 Sanchez, I. C. and Eby, R. K. *Macromolecules* 1975, **8**, 639
45 Sanchez, I. C. *J. Polym. Sci., Polym. Symp.* 1977, **59**, 109
46 Colson, J. P. and Eby, R. K. *J. Appl. Phys.* 1966, **37**, 3511
47 Fischer, E. W., Sterzel, H. J. and Wegner, G. *Kolloid Z. Z. Polym.* 1973, **251**, 980
48 Wunderlich, B. 'Macromolecular Physics', Vol. 1, 'Crystal Structure, Morphology, Defects', Academic Press, New York, 1973